doi:10.1016/j.jmb.2005.06.075 J. Mol. Biol. (2005) 352, 11–21

JMB

Available online at www.sciencedirect.com

SCIENCE DIRECT®

ELSEVIER

COMMUNICATION

A Structural Basis for Depolymerization of Alginate by Polysaccharide Lyase Family-7

Masayuki Yamasaki[1], Kohei Ogura[2], Wataru Hashimoto[2] Bunzo Mikami[1]† and Kousaku Murata[2]*†

[1]*Division of Agronomy and Horticultural Science, Graduate School of Agriculture, Kyoto University, Uji, Kyoto 611-0011 Japan*

[2]*Division of Food Science and Biotechnology, Graduate School of Agriculture, Kyoto University, Uji, Kyoto 611-0011 Japan.*

**Corresponding author*

Alginate lyases depolymerize alginate, a heteropolysaccharide consisting of α-L-guluronate and β-D-mannuronate, through a β-elimination reaction. Their structure/function relationships are expected to provide information valuable to future industrial alginate processing and drug design for *Pseudomonas aeruginosa* alginate biofilm-dependent infection, but much remains unknown. Here, we present the crystal structure at 1.0 Å resolution and the results of mutational analysis of *Sphingomonas* sp. A1 alginate lyase A1-II′, which is grouped into the polysaccharide lyase (PL) family-7. The overall structure of A1-II′ uses a β-sandwich fold, and it has a large active cleft covered by two short flexible loops. Comparison with other family PL-7 structures indicated that loop opening is necessary for substrate binding when the catalytic reaction is initiated. In contrast to the disorder in many side-chains on the protein surface, the three adjacent β-strands at the center of the active cleft are well ordered. This results from hydrogen bond networks and stacking-like associations identical with those in other family PL-7 structures. Disruption of these interactions by site-directed mutagenesis (R146A, E148A, R150A, Q189A, and K280A) makes the protein insoluble or greatly decreases its activity. The A1-II′ structure includes two sulfate ions in the active cleft. Ammonium sulfate was a potent inhibitor with a K_i of 2.5 mM, indicating that our structure represents a model of the inhibitory state. Results of mutational analysis and continuous hydrogen bond networks suggest that Arg146, Gln189, His191, and Tyr284 form an active center. Tyr284OH appears particularly crucial to the catalytic reaction, which is supported by sulfate ion binding and the proximity to the C5 and O4 atoms of subsite +1 in the model obtained by energy minimization calculations using tri-mannuronate. The structural basis shown by this study is similar in many respects to that of the family PL-5 enzymes.

© 2005 Elsevier Ltd. All rights reserved.

Keywords: alginate lyase; polysaccharide lyase family-7; crystal structure; active center

Alginate produced by brown seaweed is used widely in the food and pharmaceutical industries due to its ability to chelate metal ions and to form a highly viscous solution.[1,2] Alginate oligosaccharides released from alginate through the actions of lyases have been shown to function as oligosaccharins[3] such as a bifidus factor[4] and an elicitor of plant growth.[5] The production of different alginate oligosaccharides with lyases is required to aid development of a more functional alginate for industrial use. Alginate may, however, cause critical disease damage in humans. Alginate secreted by pathogenic bacteria such as *Pseudomonas aeruginosa*, for example, is known to be a component of the capsule-like biofilm responsible both for chronic

† B.M. & K.M. contributed equally to this work.

Abbreviations used: MIR, multiple isomorphous replacement.

E-mail address of the corresponding author: kmurata@kais.kyoto-u.ac.jp

0022-2836/$ - see front matter © 2005 Elsevier Ltd. All rights reserved.

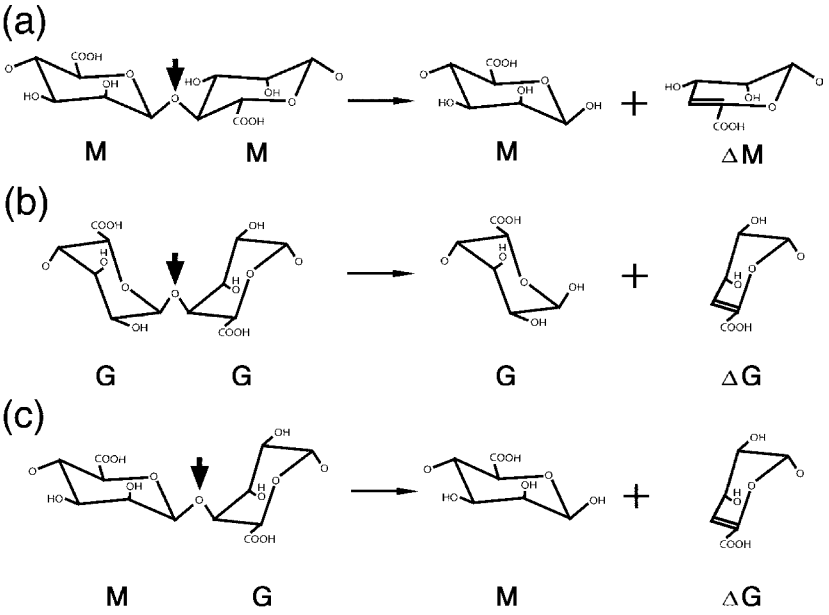

Figure 1. Block sites of alginate polymers and alginate lyase reactions. (a) MM; (b) GG; (c) MG block sites. *M* and *G* represent β-D-mannuronate and α-L-guluronate. Vertical and horizontal arrows indicate cleavage sites for alginate lyase reactions and reaction schemes.

pulmonary infection and respiratory difficulty in patients with cystic fibrosis.[6,7] It is thus important to clarify the relationship between the structure and function of alginate lyases, which may be applicable to biochemicals for the molecular design of an edible alginate or drug design for biofilm-dependent infections caused by *P. aeruginosa*. The structural basis for the alginate depolymerization mechanism remains poorly understood, however.

Alginate is a polysaccharide consisting of β-D-mannuronate and its C5 epimer, α-L-guluronate, arranged in three different blocks: poly β-D-mannuronate (poly-M), poly α-L-guluronate (poly-G), and hetero-polymeric (poly-MG) regions (Figure 1).[8] Alginate lyases depolymerize alginate through a β-elimination reaction that releases unsaturated saccharides with C=C double bonds at their non-reducing terminal uronate residues. On the basis of their primary structures, alginate lyases are now classified into four groups, i.e. polysaccharide lyase (PL) families 5, 7, 14, and 15, including some proteins whose functions are unknown†. Among these families, family PL-5 and PL-7 enzymes act on alginate polymers endolytically and produce oligosaccharides, but show some difference in diversity in substrate specificities. The substrate specificity of an alginate lyase depends on the composition, not on the type of linkage, of uronic acids in the alginate polymer.[8] Contrary to the narrow substrate specificity for poly-M of family PL-5 enzymes, family PL-7 enzymes exhibit diverse substrate specificities: *Sphingomonas* sp. A1 alginate lyase A1-II[9] and *Corynebacterium* sp. AlyPG[10] for poly-G, *Photobacterium* sp. alginate lyase AlxM[11] for poly-M, *P. aeruginosa* PA1167[12] for poly-MG, and *Sphingomonas* sp. A1 alginate lyase A1-II′, investigated here, for all substrates equally. The substrate specificity itself is not so strict; for example, *Sphingomonas* sp. A1 A1-II, which has a preference for poly-G, may act also on poly-MG, although the activity is only 20% of that toward poly-G, and PA1167 with a preference for poly-MG can act also on poly-M, the activity being 16% of that toward poly-MG.[12]

The structures of family PL-5 and PL-7 enzymes have been well studied. The family PL-5 enzyme *Sphingomonas* sp. A1 alginate lyase A1-III uses an α/α-barrel structure as a basic scaffold,[13] and is the only family PL-5 enzyme analyzed structurally in sufficient detail through substrate complex structure determination. The flexible motion of a lid loop is important in the reaction mechanism involving His192 and Tyr246 as catalytic residues, and arginine residues in the active cleft appear crucial to binding to the carboxylic acid mannuronate.[14,15] These are very important observations for evaluating the structural basis for the alginate depolymerization by family PL-5 enzymes. Family PL-7 enzymes with known structures, *P. aeruginosa* alginate lyase PA1167[12] and *Corynebacterium* sp. guluronate lyase Aly-PG,[16] use a β-sandwich structure as a basic scaffold, as shown by structure determination. Through structural analysis of family PL-7 proteins, an active cleft has been proposed on the basis of the characteristic localization of conserved residues in the tertiary structure; they are on three adjacent β-strands at the center of a large cleft (A3, A4, and A5, in line with our naming for PA1167) and conduct multiple interactions.[12] This unique structural conservation has significant implications for acting as family PL-7 enzymes. They may be involved also in unknown underlying features of the structure/function

† http://afmb.cnrs-mrs.fr/~cazy/CAZY/index.html

Table 1. MIR phasing

Derivative	$NaAuCl_4$	K_2PtCl_4
Soaking conditions	2 mM, 0.5 h	10 mM, 0.5 h
Resolution limit (Å)	3.5	3.5
No. sites	2	1
R_{cullis}	0.68	0.61
R_{kraut}	0.13	0.076
Phasing power	0.98	1.4
Mean figure of merit	0.38	
After solvent flattening	0.78	

The structure of A1-II′ was determined by multiple isomorphous replacement (MIR). A1-II′ crystals were soaked in solutions containing 2 mM $NaAuCl_4$ and 10 mM K_2PtCl_4 for 0.5 h at 20 °C. Heavy-atom solutions were prepared in 0.1 M sodium acetate (pH 4.5), 0.2 M ammonium sulfate, and 27.5% PEG 8000. Diffraction data of native crystals up to 2.0 Å and of derivative crystals around 3.5 Å were collected with a Bruker Hi-Star multiwire area detector at 7 °C, using CuKα radiation generated by an MAC Science M18XHF rotating anode generator, and were processed, merged, and scaled with the SADIE and SAINT software packages (Bruker, Karlsruhe Germany). The precession image indicated that the crystal belongs to space group $P2_12_12_1$. One molecule was included in an asymmetric unit. MIR phasing was conducted with a PHASES program package.[30] An electron density map was obtained with the solvent-flattened MIR phase using data from 15.0–3.5 Å. The initial model obtained using an averaged MIR map at 3.5 Å resolution was refined by simulated annealing with molecular dynamics using a CNS program package.[23] Then, several rounds of restrained least-squares refinement, followed by manual model building using the program Turbo-Frodo (AFMB-CNRS, France), were conducted to improve the initial model to an *R*-factor of 18.2% at 2.0 Å resolution.

Table 2. Data collection, structure refinement, and model status

Cell dimensions	
a (Å)	34.58
b (Å)	68.47
c (Å)	80.33
Space group	$P2_12_12_1$
A. *Data collection*	
Resolution (Å) (last shell)	26.1–1.00 (1.04–1.00)
No. of reflections (last shell)	921,331 (57,340)
Completeness (%) (last shell)	96.0 (76.0)
$I/\sigma(I)$ (last shell)	9.5 (4.0)
$R(I)_{merge}$ (%) (last shell)	5.3 (21.3)
B. *Structure refinement*	
Reflections with $F > 4\ \sigma$ (for R_{free})	763,642 (40,334)
Isotropic: R_{cryst}/R_{free} (%)	14.08/16.11
Anisotropic: R_{cryst}/R_{free} (%)	10.29/13.36
All reflections (for R_{free})	874,098 (45,961)
Anisotropic R_{cryst}/R_{free} (%)	11.01/14.14
C. *Model status*	
ESDs of fully occupied atomic positions	
Most ordered regions ($B < 5$ Å^2) (Å)	<0.02
Remainder of the molecule (Å)	0.04
RMSD from ideal values	
Bond lengths (Å)	0.017
Bond angles (deg.)	0.033
Ramachandran plot	
Most-favored regions (%)	89.6
Additionaly allowed regions (%)	9.8
Generously allowed regions (%)	0.5
Disallowed regions (%)	0
Mean *B*-factor (fully/partially occupied)	
Protein main-chain (876/33) (Å^2)	5.97/9.63
Protein side-chain (749/78) (Å^2)	7.49/9.72
Sulfate ion (0 /10) (Å^2)	n. d./8.97
Glycerol (0/6) (Å^2)	n. d./25.27
Solvent (373/38) (Å^2)	22.10/17.71

Diffraction data for the following refinement was collected in a resolution range of 50–1.0 Å using synchrotron radiation of wavelength 0.7 Å at the BL-38B1 station of SPring-8, Hyogo, Japan, as described.[19] Data obtained were processed, merged, and scaled using the HKL2000 program package (DENZO and SCALEPACK),[31] and truncated with the CCP4 program package. Starting from the initial model obtained through MIR phasing, the structure was first refined with a CNS program package, and then with a SHELXL program package by isotropic refinement,[32] followed by anisotropic refinement. Several rounds of restrained least-squares refinement to a resolution of 1.0 Å, followed by manual modeling were conducted to improve the model, until no peak higher than 5 σ was seen in a $F_o - F_c$ map. The stereoquality of the model was assessed using the SHEXL, PROCHECK,[33] and WHAT-CHECK programs.[34] Leu308 fell into the generously allowed regions on a Ramachandran plot, which would have resulted from the great flexibility of the His-tag residues at the C terminus.

relationships of family PL-7 enzymes; for example, the nature of catalytic residues and how they bind substrates.

Probing the structural basis of family PL-7 is interesting also for determining structural similarities to family PL-5 enzymes. They are already known to have different basic frameworks, but they act endolytically on the same substrate, alginate polymer. Considering other PL families, families PL-1 and PL-10 show a surprising similarity in the disposition of active center residues and catalytic mechanism, despite the topological difference

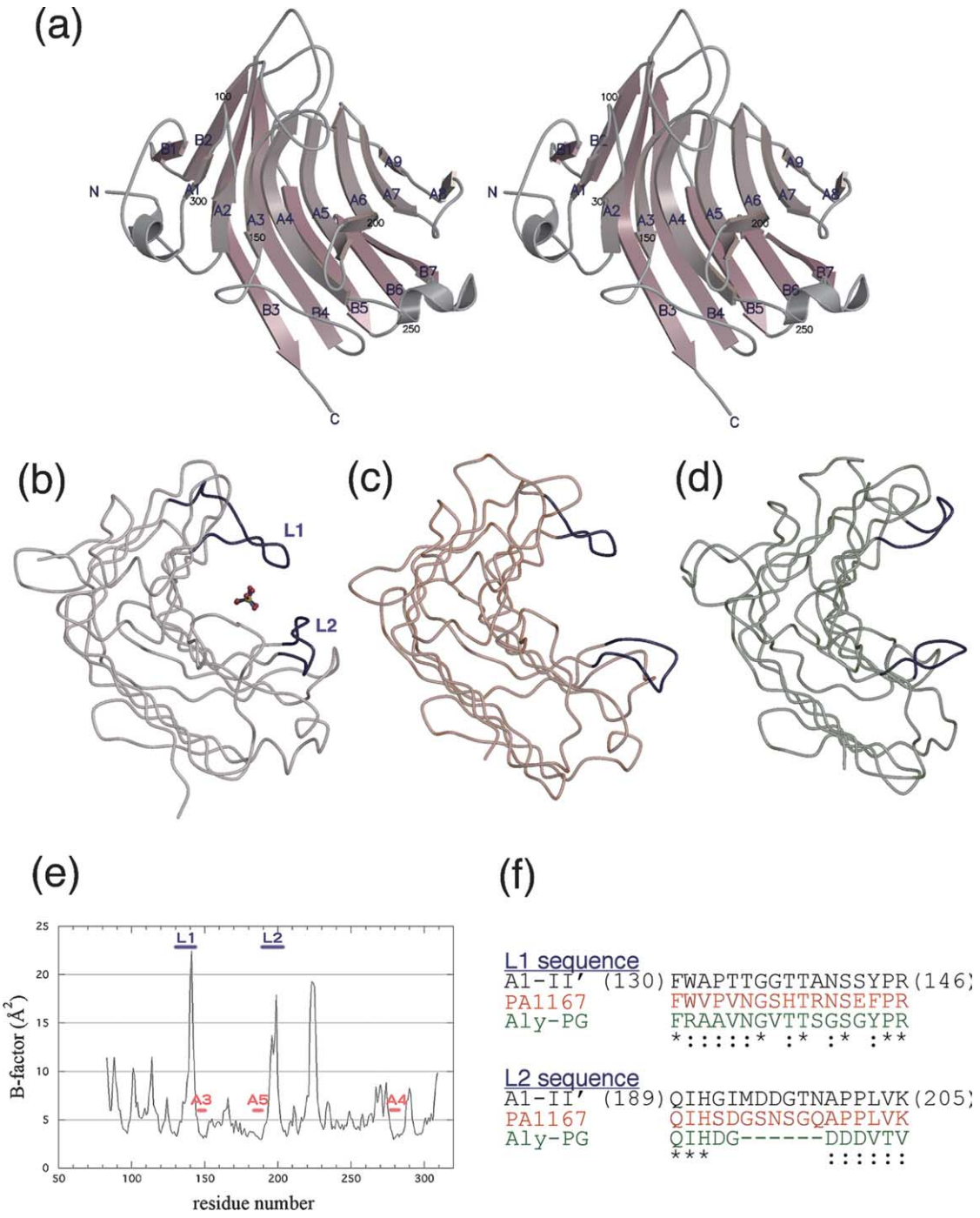

Figure 2. Overall structure of family PL-7 enzymes and implications for loop motion. (a) Ribbon stereodiagram of alginate lyase A1-II′ from *Sphingomonas* sp. A1. β-Sheet A (1–9) is shown in grey and β-sheet B (1–7) in pink. (b) C^{α} trace of A1-II′ with sulfate ions. L1 and L2 loops are shown in dark blue. (c) C^{α} trace of *P. aeruginosa* PA1167 (PDB code 1VAV). (d) C^{α} trace of *Corynebacterium* sp. Aly-PG (PDB code 1UAI). (e) *B*-value plots of A1-II′. (f) Structure-based alignment of the L1 and L2 loop sequence of A1-II′, PA1167 and Aly-PG. Structures were superimposed using the TURBO/rigid2 program. Identical and similar amino acid residues are denoted by asterisks and dots. The Figures were prepared using the programs MOLSCRIPT[28] and Raster3D.[29]

between β-helix (family PL-1) and α/α-barrel (family PL-10) structures.[17] It is thus natural to consider that some similarities exist in the catalytic mechanism of PL-5 and PL-7 enzymes.

In a previous study of *P. aeruginosa* PA1167, we tried to determine the structural basis for the depolymerization of alginate by family PL-7 enzymes, but it was difficult because the enzyme activity was extremely weak. We recently identified alginate lyase A1-II′ from *Sphingomonas* sp. A1 as a suitable enzyme, although the biological aspects of A1-II′ remain unknown; A1-II′ was first found as a hypothetical protein by homology analysis with alginate lyase A1-II against the genome database of *Sphingomonas* sp. strain A1, and showed no expression in bacterial cells.[18] A1-II′ exhibits significant enzyme activity distinct from that of *P. aeruginosa* PA1167,[18] forming fine crystals suitable for obtaining atomic resolution data.[19] In the present study, we determined the atomic structure of alginate lyase A1-II′ at 1.0 Å resolution. Through mutational analysis of conserved residues, we then determined how they contribute to the structure and function of family PL-7 enzymes. We evaluated structural similarity at the active site with family PL-5 A1-III, and deduced the structural basis for the catalytic mechanism by energy minimization calculations using a model of tri-mannuronate from family PL-5 A1-III.

Overall structure with a β-sandwich fold

The recombinant protein of *Sphingomons* sp. A1 alginate lyase A1-II′ was purified from a cell extract of *Escherichia coli* transformant with plasmid pET21b/A1-II′ of BL21(DE3), and then crystallized.[19] The A1-II′ structure was determined initially by multiple isomorphous replacement (MIR), using data for gold and platinum derivatives collected with a laboratory source. Phasing statistics are given in Table 1. The initial model was further improved using synchrotron data obtained at SPring-8 (Hyogo, Japan), and finally the structure was refined at 1.0 Å resolution with an R value of 10.29% after anisotropic refinement using $F > 4\sigma$ data. Data collection and refinement statistics are given in Table 2. The final model consisted of 227 amino acid residues, two sulfate ions, one glycerol molecule, and 411 water molecules. Many alternate structures were observed on 18 side-chain orientations of Lys, Gln, Asn, Asp, Met, Leu, and Ile residues, on three main-chains of Gly, Asn, and Pro residues, and on one sulfate ion, almost all of which are located at the protein surface. Partial structures determined by occupancy refinement were observed on one sulfate ion and some water molecules.

The overall structure of A1-II′ is a glove-like β-sandwich fold (Figure 2(a)) composed of four short helices and two large β-sheets. Sheet A consists of nine β-strands, A1 (residues 104–106), A2 (94–97), A3 (146–151), A4 (276–285), A5 (185–193), A6 (199–209), A7 (212–218), A8 (226–228), and A9 (231–233), and sheet B consists of seven β-strands, B1 (120–122), B2 (128–133), B3 (294–307), B4 (167–178), B5 (241–248), B6 (251–256), and B7 (259–264), all of which use an antiparallel arrangement, except that a break occurs in the β-structure in the connecting loop between A8 and A9. *P. aeruginosa* PA1167[12] and *Corynebacterium* sp. Aly-PG[16] also have a β-sandwich structure, and are well superimposed on A1-II′ with an rmsd of 0.568 Å (113 C^{α} atoms) and 0.588 Å (120 C^{α} atoms). The glove-like β-sandwich is a common fold in family PL-7 enzymes.

Characteristic loop motion for substrate binding

Two sulfate ions are found above strands A3 and A5 in the cleft. Seen along the axis that binds them, the clearly visible tunnel is presumed to play a crucial role in the enzyme action (Figure 2(b)). However, a tunnel-type conformation is generally used by *exo*-type polysaccharide lyases and hydrolases, whose reaction is processive.[20,21] Family PL-7 enzymes, including A1-II′, are all *endo*-type lyases, and substrate alginate is a huge polymer; the average molecular mass of sodium alginate (Nacalai Tesque Co., Ltd) that we usually use in a reaction assay is about 26 kDa, corresponding to a 140mer, so it is plausible to assume that the sides of the substrate binding tunnel would be flexible and open to permit binding of the substrate in the middle of a long chain. The *B*-factor plots of all C^{α} atoms showed that three flexible regions exist (Figure 2(e)), a loop connecting strands B2 and A3 (L1, 130–145), a loop from the end of strand A5 to the middle of strand A6 (L2, 190–203), and a loop connecting strands A7 and A8 (219–225). PA1167 and Aly-PG have similar L1 and L2 loops above the active cleft (Figure 2(c) and (d)). In structure-based alignment, the L1 loop showed a high level of sequence similarity among all enzymes (Figure 2(f)). Aly-PG appears to use an open conformation, unlike the closed conformation of other enzymes. The L2 loop showed a high level of sequence similarity between A1-II′ and PA1167, and PA1167 appears to use an open conformation. These observations support the view that loop motion is necessary for substrate binding by family PL-7 enzymes, although it is still difficult to determine the contribution of each of the L1 and L2 loops. A1-II′ may be a cleft-type enzyme with two flexible loops, L1 and L2, that cover the active cleft and form a tunnel.

Contribution of conserved residues to family PL-7 enzyme structures

The active cleft is extremely well ordered, there being no disordered structures, and the mean *B*-factor for C^{α} atoms in A3, A4, and A5 is 3.93 $Å^2$ (Figure 2(e)). Residues conserved in family PL-7 enzymes are localized on strands A3, A4, and A5 in the active cleft. Of these, residues on the protein surface consist of Arg146, Glu148, and Arg150 of the

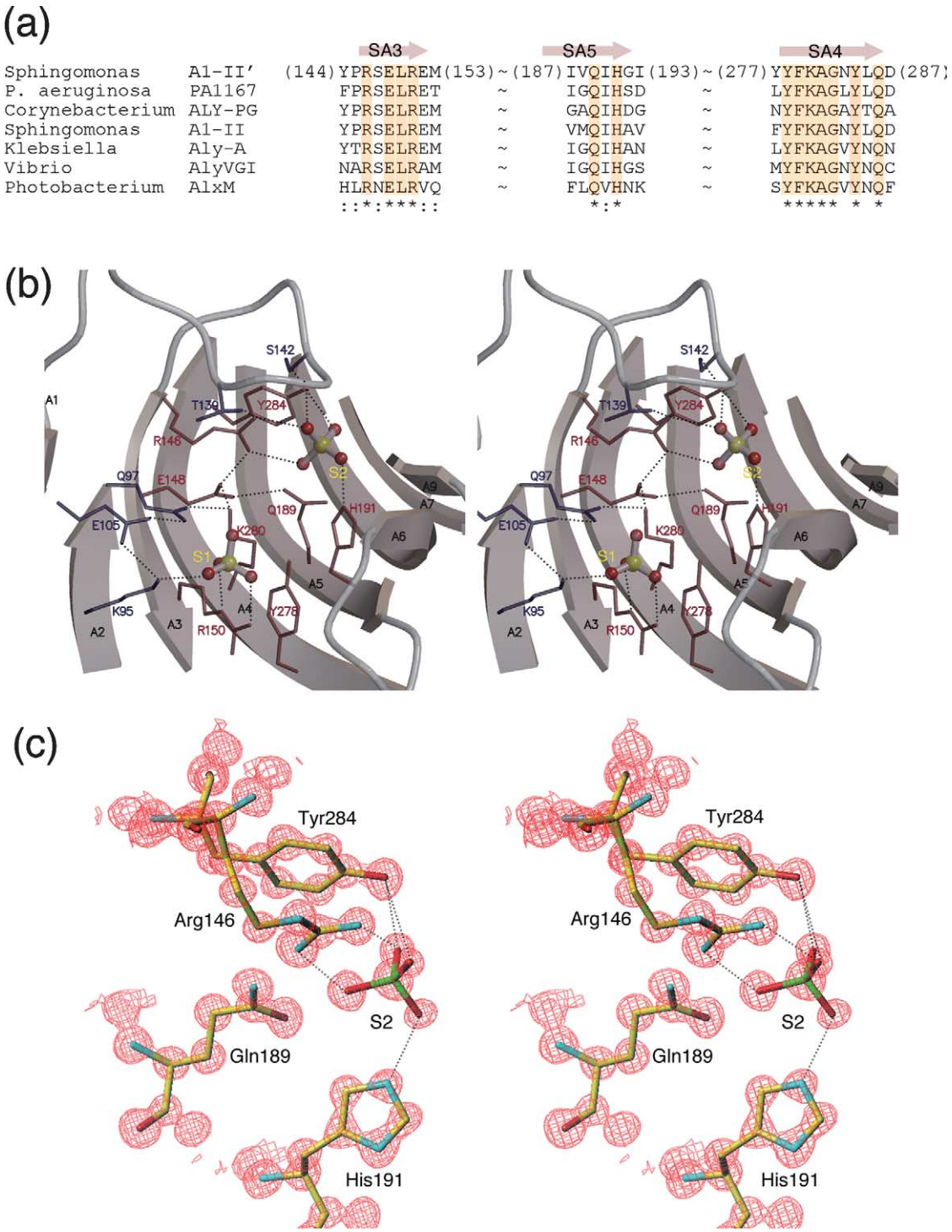

Figure 3. Active cleft structure. (a) Alignment of the amino acid sequences conserved in family PL-7 alginate lyases using the ClustalW program (clustalw.genome.ad.jp/). Sphingomonas A1-II′ (accession number AB120939) of *Sphingomonas* sp. A1; P. aeruginosa PA1167 (accession number AE004547) of *P. aeruginosa* PAO1; Corynebacterium Aly-PG (accession number AB030481) of *Corynebacterium* sp. ALY-1; Sphingomonas A1-II (accession number AB011415) of *Sphingomonas* sp. A1; Klebsiella AlyA (accession number L19657) of *K. pneumoniae* subsp. *aerogenes*; Vibrio AlyVGI (accession number AF114039) of *Vibrio halioticoli* IAM14596T; and Photobacterium AlxM (accession number X70036) of *Photobacterium* sp. ATCC 43367. Identical and similar amino acid residues in the seven kinds of alginate lyases are denoted by asterisks and dots. Secondary structure elements of A1-II′ are shown as above. (b) Hydrogen bond networks in active cleft with two sulfate ions. Conserved residues are shown as brown bonds and other residues participating in networks as dark blue bonds. Sulfate ions are shown as ball-and-stick models. To simplify the description, S1 is shown in a single conformation with greater occupancy. (c) Active center structure. Arg146, Gln189, His191, Tyr284, and sulfate ion S2 were described with the $2F_o - F_c$ map contoured at 2.5 σ. C, O, N, and S atoms are shown as yellow, red, blue, and green, respectively. This Figure was prepared using Turbo-Frodo.

four conserved residues on strand A3, Tyr278, Lys280, Gly282, Tyr284, and Gln286 of the seven conserved residues on strand A4, and Gln189 and His191 of all those on strand A5 (Figure 3(a)).

Along the active cleft, continuous hydrogen bond networks are formed among conserved residues, non-conserved residues, and two sulfate ions (Figure 3(b)). The three hydrogen bonds, including two charged ones, are as follows: Arg146NH1–Glu148OE1 (2.84 Å), Glu148OE2–Gln189NE2 (2.94 Å), and Glu148OE1–Lys280NZ (2.69 Å) (Figure 3(b)). More characteristic interactions are the two sets of stacking-like interactions between Tyr284 and Arg146, and between Try278 and Arg150; the benzene ring plane of the tyrosine residue and the plane formed by NH1, NH2, CZ, and NE of the arginine residue are almost parallel at 3.5 Å (Figure 3(b)). In addition to the overall structural similarity to PA1167 and Alg-PG, A1-II′ is well superimposed on strands A3, A4, and A5 with PA1167 (rmsd = 0.227 Å, for all C^{α} atoms in strands A3, A4, and A5) and with Aly-PG (rmsd = 0.192 Å). The side-chain orientations are very similar, indicating that characteristic interactions of conserved residues are shared by family PL-7 enzymes. All of these observations suggest the importance of structural rigidity in strands A3, A4, and A5 for the action of family PL-7 enzymes.

To verify this importance, we conducted mutational analysis. Mutants of R146A, E148A, R150A, Q189A, H191A, Y278F, K280A, and Y284F were prepared and their kinetic parameters examined (Table 3). All mutants except for Y278F showed large decreases in V_{max}. It appears difficult to understand the result completely, but we should first consider the effect of the disruption of hydrogen bond networks on the accurate construction of the active cleft. Glu148, Gln189, and Lys280 are located at the bottom of the active cleft and form continuous hydrogen bond networks with surrounding residues (Figure 3(b)). Their replacement would greatly affect protein folding itself, resulting in the insolubility of E148A, great increases in K_m, and significant decreases in V_{max} of Q189A and K280A. The two sets of stacking-like interactions would be disrupted by the mutation of R146A and R150A. K_m did not change significantly compared to the great decreases in V_{max}. This would result from an improper binding of substrate; in other words, a non-productive binding. Binding of long-chain substrates such as alginate requires many binding sites. From the substrate model of enzyme for polymer substrate,[22] significant loss of V_{max} would be observed when the ratio of non-productive to productive binding increased significantly. If the sum of both bindings is not so different from that of wild-type, the change in K_m is small. All results support the importance of the structural rigidity of strands A3, A4, and A5 in the action of the A1-II′ enzyme.

Other mutations are thought to have only negligible effects on the structural rigidity of the active cleft, because His191 exhibits no clear interaction with the surrounding residues (Figure 3(b)), and replacing tyrosine with phenylalanine causes only deletion of an OH group. Increases in K_m of mutants H191A, Y278F, and Y284F may result directly from the loss of interactions on binding with a substrate. Mutations of H191A and Y284F caused significant decreases in V_{max}, in contrast to the small increase for Y278F, indicating the involvement of His191 and Tyr284 residues in the catalytic reaction.

Structural conservation in strands A3, A4, and A5 thus implies the significance of the rigidity of the active cleft, the binding of the substrate, and

Table 3. Kinetic parameters of A1-II′ mutants

	K_m (μg/ml)	V_{max} (min^{-1})	
Wild-type	1.51 ± 0.25	46.27 ± 1.71	(100)[a]
+ $(NH_4)_2SO_4$	30.85 ± 0.81[b]	48.16 ± 1.17[b]	(104)
R146A	1.24 ± 0.061	0.24 ± 0.0023	(0.52)
E148A	n.d.[c]	n.d.	
R150A	2.9 ± 0.79	0.022 ± 0.015	(0.047)
Q189A	24.04 ± 9.14	0.00025 ± 0.000033	(0.00054)
H191A	4.3 ± 1.21	0.0064 ± 0.00058	(0.014)
Y278F	5.9 ± 0.53	57.89 ± 2.18	(125.24)
K280A	8.63 ± 2.38	0.019 ± 0.0017	(0.042)
Y284F	6.86 ± 1.04	0.15 ± 0.079	(0.31)

A1-II′ showed a great increase in K_m on the addition of 37 mM ammonium sulfate, indicating that it inhibits A1-II′ competitively. K_i was determined as 2.5(±0.072) mM. The site-directed mutagenesis of A1-II′ was conducted by the QuikChange method using plasmid pET21b/A1-II′. All mutants except for E148A were expressed as a soluble protein in the cell extract of *E. coli*, purified by the same method as that used for the wild-type, and confirmed by far-UV CD spectral analysis (190–250 nm) with a J-720 (Jasco, Japan) spectrometer to fold into the native form, i.e. an abundant β-structure, as seen in the wild-type protein. Each enzyme was incubated at 30 °C in a reaction mixture containing 50 mM Tris–HCl (pH 7.5) and different concentrations of alginate. Enzyme activity was determined by measuring the increase in absorbance at 235 nm due to the double bond formed in the reaction product. The protein content was determined by measuring absorbance at 280 nm, assuming that $E_{280} = 1.0$ corresponds to 1 mg/ml of protein. Kinetic parameters were determined by non-linear fitting with the program KaleidaGraph.

[a] V_{max} relative to that of the wild-type (%).

[b] These are apparent K_m and V_{max} on inhibition by sulfate ion.

[c] The mutant protein is insoluble.

the catalytic reaction itself. To further examine the catalytic mechanism of family PL-7 enzymes, we must study the active cleft in detail.

Sulfate ions binding to the active center

Along the active cleft, continuous hydrogen bond networks are formed among conserved residues, non-conserved residues, and two sulfate ions (Figure 3(b)). Sulfate ion S1 is located above strand A3 with two conformations, whose main structure (Figure 3(b)) was refined to an occupancy of 0.58. S1 is held by Lys95 (NZ-O2, 2.83 Å) and Arg150 (NE-O1, 2.83 Å; NH2-O3, 2.91 Å) at the end of hydrogen bond networks starting from Arg146 to Glu148, Glu97, and Glu105, whose interactions differ slightly in the substructure. S2 is located above strand A5 with a single conformation but is partially occupied, with refinement to an occupancy of 0.66. S2 is held by Arg146 (NH1-O1, 2.96 Å; NH2-O4, 2.85 Å), His191 (NE2-O2, 2.55 Å), and Tyr284 (OH-O3, 2.71 Å; OH-O4, 3.15 Å). These sulfate ions are derived from ammonium sulfate in the crystallization buffer, and thus bind to the active cleft of A1-II′. All crystallization conditions we studied involved a significant amount of ammonium sulfate, which would stabilize the protein conformation and lead to crystallization. Kinetic analysis have shown that ammonium sulfate inhibits A1-II′ competitively with $K_i = 2.5$ mM (Table 3), indicating that our structure represents a model of the inhibitory state.

Interestingly, S2 binds to His191 and Tyr284, both of which have been identified by mutational analysis to be important in the catalytic reaction. For family PL-5 A1-III, histidine and tyrosine residues are important to the catalytic mechanism,[14,15] so it is reasonable to assume that His191 and Tyr284 for an active center with surrounding residues, Arg146 and Gln189 (Figure 3(c)), and binding of S2 represents the inhibition, although the occupancy of S2 was refined as 0.66. In the mutational analysis, R146A and Q189A were thought to disrupt hydrogen bond networks in the active cleft and to operate disadvantageously on the construction of the active center itself, so it remains

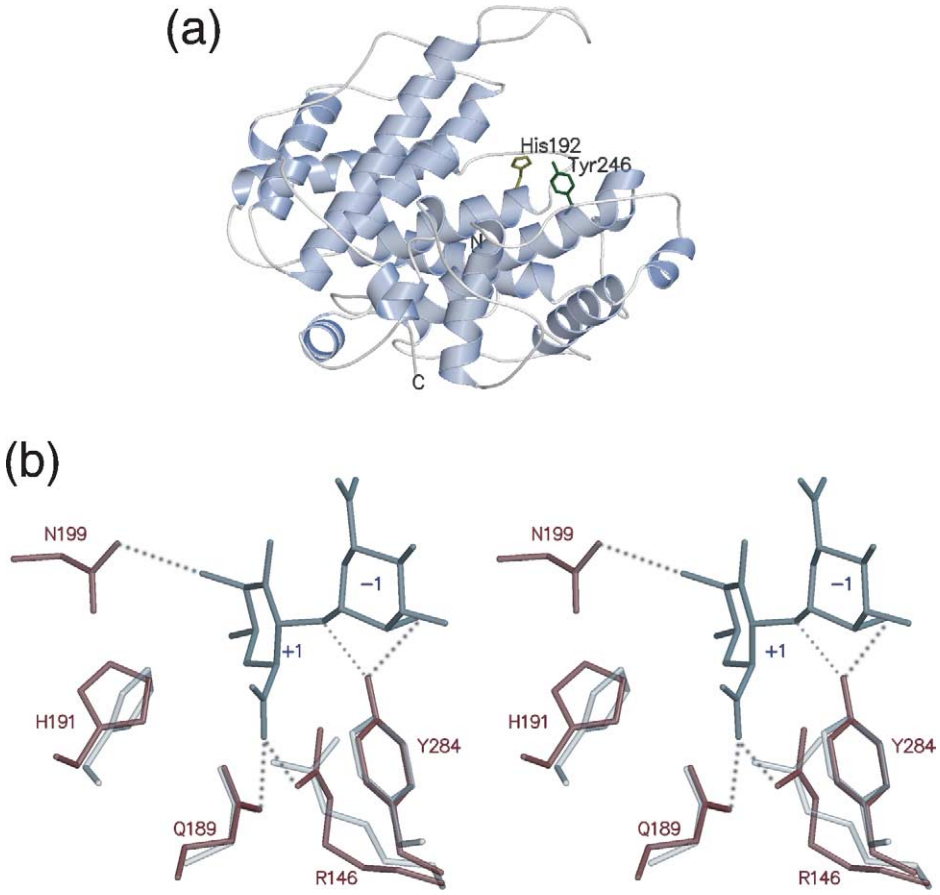

Figure 4. Implication for catalytic mechanism. (a) Ribbon diagram of family PL-5 alginate lyase A1-III from *Sphingomonas* sp. A1. Catalytic residues are shown as bonds. (b) Substrate binding model (stereodiagram) obtained by energy minimization calculations using the model of tri-mannuronate from the substrate complex structure of family PL-5 A1-III. The A1-II′ residues Arg146, Gln189, His191, and Tyr284, shown in brown, superimposed well on the A1-III residues Arg239, Asn191, His192, and Tyr246, shown in gray. To simplify the description, subsites +1 and −1 are shown in blue.

unclear whether these residues participate in the catalytic mechanism. It is interesting that S2 forms hydrogen bond networks with Ser142 of the L1 loop through Tyr284OH, which also involves Thr139 through Arg146. The L1 loop may assist the depolymerization of alginate by A1-II′ in the catalytic reaction or binding of the substrate.

Unique similarity of family PL-5 and PL-7 enzymes

Family PL-5 lyases have an α/α-barrel as a basic scaffold, which shows the difference in amino acid sequence and overall structure from that of family PL-7 enzymes (Figure 4(a)). The structural properties we found in this study are similar to those of family PL-5 enzymes. Loop motion is one of the characteristic features that show family PL-5 A1-III has a lid loop involved in substrate binding and the catalytic reaction.[15] Mutational studies have shown that His192 and Tyr246 are crucial to catalytic reactions.[15] Active center residues of family PL-5 and PL-7 enzymes superimpose well: Arg239, Asn191, His192, and Tyr246 of A1-III on Arg146, Gln189, His191, and Tyr284 of A1-II′ (Figure 4(b)). This similarity is observed also between family PL-1 and PL-10 enzymes; six residues are disposed identically in the active center, despite the topological difference between the β-helix of family PL-1 and the α/α-barrel of family PL-10.[17] Family PL-1 and PL-10 lyases were shown to have similar catalytic mechanisms.[17] To deduce the catalytic mechanism of family PL-7 enzymes, we performed energy minimization calculations with CNS software programs,[23] using the model of tri-mannuronate on family PL-5 A1-III (unpublished results).

Structural speculation on the catalytic mechanism

A1-II′ has so diverse a substrate specificity that it acts on poly-mannuronate, as A1-III does. Subsites are usually labeled so that −n represents the non-reducing end and n the reducing end, and cleavage occurs between the −1 and +1 sites.[24] In the substrate complex of A1-III, tri-mannuronate was located between subsites +1 and −2. Active site residues of A1-II′ were superimposed on that of A1-III (Figure 4(b)), then the tri-mannuronate model in A1-III was incorporated into the A1-II′ structure. The final coordinates of tri-mannuronate were determined after energy minimization calculation for 100 cycles

The enzymatic reaction of alginate lyase starts with the abstraction of the C5 proton at subsite +1 by a general base, and finishes with the proton donation to the O4 atom at subsite +1 by a general acid.[8] In this model, distances from the C5 atom of subsite +1 to the surrounding atoms of A1-II′ are 3.68 Å to Arg146NH2, 4.09 Å to His191NE2, and 2.84 Å to Tyr284OH. In mutational analysis, H191A activity decreased significantly, and in the reaction mechanism of family PL-8 hyaluronate lyase, it has been proposed that the histidine residue works as a general base.[25] In A1-II′, however, it is too far for His191NE2 to abstract the C5 proton, so, on the basis of structural distances, Tyr284 is a plausible candidate for a general base., Tyr284OH is the only atom close to the O4 atom at 2.54 Å, so Tyr284 is also a candidate for a general acid. This bi-functional nature of the tyrosine residue in the lyase reaction has been proposed for alginate lyase A1-III (family PL-5),[14,15] xanthan lyse (family PL-8),[26] and chondroitin AC lyase (family PL-8).[27]

What role does His191 have in the catalytic reaction of A1-II′? The distance from His191NE2 to subsite +1 atoms is 3.63 Å to O5, 3.47 Å to O61, and 4.00 Å to O62. Viewing other interactions between a protein and subsite +1, Asn199ND2 interacts with O2 by 2.83 Å, Arg146NH1 with O62 by 2.69 Å, and Gln189NE2 with O62 by 2.80 Å. Considering the structural evidence together with other studies of PL enzymes,[14,15,25–27] we deduced three possibilities about the role of His191. (i) It keeps the substrate at the optimal position for the next catalytic reaction with surrounding Asn199 from loop L2, Arg146, and Gln189; subsite +1 in particular has many interactions compared to that of subsite −1 (O2–Tyr284OH, 2.93 Å) and subsite −2 (O62–Tyr144OH, 3.13 Å). (ii) In the underlying assumption about the proton abstraction of C5 proton by Tyr284OH, it neutralizes the negative charge on C5 carboxylate groups together with Arg146 and Gln189. (iii) It stabilizes a carboxylate dianion intermediate before proton donation to the O4 atom by Tyr284OH. This structural basis for the catalytic mechanism deduced by this study remains inconclusive and should be examined further by the combination of mutational analysis and structural determination with substrate or substrate analogs.

Protein Data Bank accession number

The atomic coordinates of alginate lyase A1-II′ at 1.0 Å resolution have been deposited in the RCSB Protein Data Bank under accession number 2CWS.

Acknowledgements

This work was supported, in part, by grants-in-aid of the National Project on Protein Structure and Functional Analysis from the Ministry of Education, Culture, Sports, Science and Technology of Japan, and by the Program for the Promotion of Basic Research Activities for Innovative Biosciences (PROBRAIN) of Japan. We thank Drs H. Sakai and K. Hasegawa of the Japan Synchrotron Radiation Research Institute (JASRI) for their kind help in data collection. X-ray data collection at BL38B1 of SPring-8 was conducted with the approval of the

organizing committee of SPring-8 (proposal no. 2004B0851-NL1-np-P3K, BM).

References

1. Onsøyen, E. (1996). Commercial applications of alginates. *Carbohydr. Eur.* **14**, 26–31.
2. Thomas, S. (2000). Alginate dressings in surgery and wound management: part 1. *J. Wound Care*, **9**, 56–60.
3. Darvill, A., Bergmann, C., Cervone, F., De Lorenzo, G., Ham, K. S., Spiro, M. D. *et al*. (1994). Oligosaccharins involved in plant growth and host-pathogen interactions. *Biochem. Soc. Symp.* **60**, 89–94.
4. Akiyama, H., Endo, T., Nakakita, R., Murata, K., Yonemoto, Y. & Okayama, K. (1992). Effect of depolymerized alginates on the growth of bifidobacteria. *Biosci. Biotech. Biochem.* **56**, 355–356.
5. Yonemoto, Y., Tanaka, H., Yamashita, T., Kitabatake, N., Ishida, Y., Kimura, A. & Murata, K. (1993). Promotion of germination and shoot elongation of some plants by alginate oligomers prepared with bacterial alginate lyase. *J. Ferment. Bioeng.* **75**, 68–70.
6. Batten, J. C. & Matthew, D. J. (1983). Cystic fibrosis. In *The Respiratory System* (Hodson, M. E., Norman, A. P. & Batten, J. C., eds), pp. 105–131, Oxford University Press, London.
7. Boat, T. F., Beadet, A. L. & Welsh, M. J. (1989). Cystic fibrosis. In *The Metabolic Basis of Inherited Disease* (Seriver, C. R., ed.), pp. 2649–2680, Academic Press, New York.
8. Gacesa, P. (1988). Alginates. *Carbohydr. Polym.* **8**, 161–182.
9. Yoon, H.-J., Hashimoto, W., Miyake, O., Mikami, B. & Murata, K. (2000). Overexpression in *Escherichia coli*, purification, and characterization of *Sphingomonas* sp. A1 alginate lyases. *Protein Expr. Purif.* **19**, 84–90.
10. Matsubara, Y., Kawada, R., Iwasaki, K., Oda, T. & Muramatsu, T. (1998). Extracellular poly (α-L-guluronate) lyase from *Corynebacterium* sp.: purification, characteristics, and conformational properties. *J. Protein Chem.* **17**, 29–36.
11. Malissard, M., Duez, C., Guinand, M., Vacheron, M. J., Michel, G., Marty, N. *et al*. (1993). Sequence of a gene encoding a (poly ManA) alginate lyase active on *Pseudomonas aeruginosa* alginate. *FEMS Microbiol. Letters*, **110**, 101–106.
12. Yamasaki, M., Moriwaki, S., Miyake, O., Hashimoto, W., Murata, K. & Mikami, B. (2004). Structure and function of a hypothetical *Pseudomonas aeruginosa* protein PA1167 classified into family PL-7. *J. Biol. Chem.* **279**, 31863–31872.
13. Yoon, H.-J., Mikami, B., Hashimoto, W. & Murata, K. (1999). Crystal structure of alginate lyase A1-III from *Sphingomonas* species A1 at 1.78 Å resolution. *J. Mol. Biol.* **290**, 505–514.
14. Yoon, H.-J., Hashimoto, W., Miyake, O., Murata, K. & Mikami, B. (2001). Crystal structure of alginate lyase A1-III complexed with a trisaccharide product at 2.0 Å resolution. *J. Mol. Biol.* **307**, 9–16.
15. Mikami, B., Suzuki, S., Yoon, H.-J., Miyake, O., Hashimoto, W. & Murata, K. (2002). X-ray structural analysis of alginate lyase A1-III mutants/substrate complexes: activation of a catalytic tyrosine residue by a flexible lid loop. *Acta Crystallog. sect. A*, **58**, C271.
16. Osawa, T., Matsubara, Y., Muramatsu, T., Kimura, M. & Kakuta, Y. (2005). Crystal structure of the alginate (poly α-L-guluronate) lyase from *Corynebacterium* sp. at 1.2 Å resolution. *J. Mol. Biol.* **345**, 1111–1118.
17. Charnock, S. J., Brown, I. E., Turkenburg, J. P., Black, G. W. & Davies, G. D. (2002). Convergent evolution sheds light on the anti-β-elimination mechanism common to family 1 and 10 polysaccharide lyases. *Proc. Natl Acad. Sci. USA*, **99**, 12067–12072.
18. Miyake, O., Ochiai, A., Hashimoto, W. & Murata, K. (2004). Origin and diversity of alginate lyases of families PL-5 and PL-7 in *Sphingomonas* sp. strain A1. *J. Bacteriol.* **189**, 2981–2986.
19. Yamasaki, M., Ogura, K., Moriwaki, S., Hashimoto, W., Murata, K. & Mikami, B. (2005). Crystallization and preliminary X-ray analysis of alginate lyases A1-II and A1-II′ from *Sphingomonas* sp. A1. *Acta Crystallog. sect. F*, **61**, 288–290.
20. Davis, G. & Henrissat, B. (1995). Structure and mechanism of glycosyl hydrolases. *Structure*, **15**, 853–859.
21. Divne, C., Ståhlberg, J., Teeri, T. T. & Jones, A. (1998). High-resolution crystal structures reveal how a cell cellulose chain is bound in the 50 Å long tunnel of cellobiohydrolase I from *Trichoderma reesei*. *J. Mol. Biol.* **275**, 309–325.
22. Natarajan, S. K. & Sierks, M. R. (1997). Minimizing nonproductive substrate binding: a new look at glucoamylase subsite affinities. *Biochemistry*, **36**, 14946–14955.
23. Brünger, A. T., Adams, P. D., Clore, G. M., DeLano, W. L., Gros, P., Grosse-Kunstleve, R. W. *et al*. (1998). Crystallography & NMR system (CNS): a new software system for macromolecular structure determination. *Acta Crystallog. sect. D*, **54**, 905–921.
24. Davis, G. J., Wilson, K. S. & Henrissat, B. (1997). Nomenclature for sugar-binding subsites in glycosyl hydrolases. *Biochem. J.* **321**, 557–559.
25. Jedrzejas, M. J., Mello, L. V., De Groot, B. L. & Li, S. (2002). Mechanism of hyaluronan degradation by *Streptococcus pneumoniae* hyaluronate lyase. *J. Biol. Chem.* **277**, 28287–28297.
26. Maruyama, Y., Hashimoto, W., Mikami, B. & Murata, K. (2005). Crystal structure of Bacillus sp. GL1 xanthan lyase complexed with a substrate: Insights into the enzyme reaction mechanism. *J. Mol. Biol.* **350**, 974–986.
27. Lunin, V. V., Li, Y., Linhardt, R. J., Miyazono, H., Kyogashima, M., Kaneko, T. *et al*. (2004). High-resolution crystal structure of *Arthrobacter aurescens* chondroitin AC lyase: an enzyme-substrate complex defines the catalytic mechanism. *J. Mol. Biol.* **337**, 367–386.
28. Kraulis, P. J. (1991). MOLSCRIPT: a program to produce both detailed and schematic plots of protein structures. *J. Appl. Crystallog.* **24**, 946–950.
29. Merritt, A. E. & Murphy, M. E. P. (1994). Raster3D version 2.0. a program for photorealistic molecular graphics. *Acta Crystallog. sect. D*, **50**, 869–873.
30. Furey, W. & Swaminathan, S. (1997). PHASE-95: a program package for the processing and analysis of diffraction data from macromolecules. *Methods Enzymol.* **277**, 590–620.
31. Otwinowski, Z. & Minor, W. (1997). Processing of X-ray diffraction data collected in oscillation mode. *Methods Enzymol.* **276**, 307–326.
32. Sheldrick, G. M. & Schneider, T. R. (1997). Shelxl—high-resolution refinement. *Methods Enzymol.* **277**, 319–343.
33. Laskowski, R. A., MacArthur, M. W., Moss, D. S. &

Thornton, J. M. (1993). PROCHECK: a program to check the stereochemical quality of protein structures. *J. Appl. Crystallog.* **26**, 283–291.

34. Hooft, R. W., Vriend, G., Sander, C. & Abola, E. E. (1996). Errors in protein structures. *Nature*, **381**, 272.

Edited by M. Guss

(Received 28 April 2005; received in revised form 25 June 2005; accepted 29 June 2005)
Available online 18 July 2005